Journal of Non-Newtonian Fluid Mechanics 233 (2016) 13–26

Contents lists available at ScienceDirect

Journal of Non-Newtonian Fluid Mechanics

journal homepage: www.elsevier.com/locate/jnnfm

Cessation of viscoplastic Poiseuille flow in a square duct with wall slip

Yiolanda Damianou, George Kaoullas, Georgios C. Georgiou*

Department of Mathematics and Statistics, University of Cyprus, P.O. Box 20537, 1678 Nicosia, Cyprus

ARTICLE INFO

Article history:
Received 21 July 2015
Revised 3 November 2015
Accepted 10 November 2015
Available online 2 December 2015

Keywords:
Bingham plastic
Slip
Slip yield stress
Poiseuille flow
Rectangular duct
Papanastasiou regularization
Cessation

ABSTRACT

We solve numerically the cessation of the pressure-driven Poiseuille flow of a Bingham plastic under the assumption that slip occurs along the wall following a generalized Navier-slip law involving a non-zero slip yield stress. In order to avoid the numerical difficulties caused by their inherent discontinuities, both the constitutive and the slip equations are regularized by means of exponential (Papanastasiou-type) regularizations. As with one-dimensional Poiseuille flows, in the case of Navier slip (zero slip yield stress), the fluid slips at all times, the velocity becomes and remains plug before complete cessation, and the theoretical stopping time is infinite. The cessation of the plug flow is calculated analytically. No stagnant regions appear at the corners when Navier slip is applied. In the case of slip with non-zero slip yield stress, the fluid may slip everywhere or partially at the wall only in the initial stages of cessation depending on the initial condition. Slip ceases at a critical time after which the flow decays exponentially and the stopping times are finite in agreement with theory. The combined effects of viscoplasticity and slip are investigated for wide ranges of the Bingham and slip numbers and results showing the evolution of the yielded and unyielded regions are presented. The numerical results also showed that the use of regularized equations may become problematic near complete cessation or when the velocity profile becomes almost plug.

1. Introduction

We have recently solved numerically the steady-state Poiseuille flow of Herschel–Bulkley fluids in a duct of rectangular cross section under the assumption that slip occurs along the wall only if the wall shear stress, τ_w, exceeds a critical value, τ_c, known as the slip yield stress [1]. For this purpose, we employed the following slip equation

$$\begin{cases} u_w = 0, & \tau_w \le \tau_c \\ \tau_w = \tau_c + \beta u_w, & \tau_w > \tau_c \end{cases} \tag{1}$$

where u_w is the slip velocity, defined as the relative velocity of the fluid with respect to that of the wall, and β is the slip parameter, which depends on the temperature, and on the properties of the material and of the fluid/wall interface [2]. A literature review of experimental observations of slip yield stress with both Newtonian and non-Newtonian materials is provided in Ref. [3]. When the slip yield stress vanishes, Eq. (1) is reduced to the well-known Navier slip equation:

$$\tau_w = \beta u_w \tag{2}$$

The no-slip and the perfect-slip cases correspond to $\beta \to \infty$ and $\beta = 0$, respectively. In most experimental studies on various materials τ_c appears to be much lower than the yield stress τ_0 [4–6]. In general, the relative values of τ_c and τ_0 may lead to different flow regimes (see, e.g., Refs. [1,6]). In the present work, τ_c is taken equal to τ_0, as suggested by Pearson and Petrie [7], in order reduce the number of the flow regimes.

In [1], it has been demonstrated that there are four distinct regimes in steady-state Poiseuille flow in a rectangular duct, defined by three critical values of the pressure gradient. Initially no slip occurs, in the second regime slip occurs only in the middle of the wider wall, in the third regime slip occurs partially at both walls, and eventually variable slip occurs everywhere. The two intermediate partial-slip regimes collapse to one in the case of a square duct.

In order to study the combined effects of viscoplasticity and slip in this steady-state flow, Damianou and Georgiou [1] employed the Herschel–Bulkley constitutive equation. In the present work, we solve the time-dependent flow. In order to reduce the number of parameters involved we consider here the flow of a Bingham plastic in a square duct. The Bingham constitutive equation relates the viscous stress tensor $\boldsymbol{\tau}$ to the rate-of-strain tensor $\dot{\boldsymbol{\gamma}}$ as follows

$$\begin{cases} \dot{\boldsymbol{\gamma}} = \mathbf{0}, & \tau \le \tau_0 \\ \boldsymbol{\tau} = \left(\dfrac{\tau_0}{\dot{\gamma}} + \mu \right) \dot{\boldsymbol{\gamma}}, & \tau > \tau_0 \end{cases} \tag{3}$$

* Corresponding author. Tel.: +35722892612; fax: +35722895352.
E-mail address: georgios@ucy.ac.cy (G.C. Georgiou).

http://dx.doi.org/10.1016/j.jnnfm.2015.11.002
0377-0257/

where μ is the plastic viscosity, and τ and $\dot{\gamma}$ are the magnitudes of $\boldsymbol{\tau}$and $\dot{\boldsymbol{\gamma}}$, defined respectively by

$$\dot{\gamma} \equiv \sqrt{\frac{1}{2} II_{\dot{\gamma}}} = \sqrt{\frac{1}{2} \dot{\boldsymbol{\gamma}} : \dot{\boldsymbol{\gamma}}} \quad \text{and} \quad \tau \equiv \sqrt{\frac{1}{2} II_{\boldsymbol{\tau}}} = \sqrt{\frac{1}{2} \boldsymbol{\tau} : \boldsymbol{\tau}} \tag{4}$$

where the symbol II stands for the second invariant of a tensor. Finally, the rate-of-strain tensor is defined by

$$\dot{\boldsymbol{\gamma}} \equiv \nabla \mathbf{u} + (\nabla \mathbf{u})^{\mathrm{T}} \tag{5}$$

where $\mathbf{u}$ is the velocity vector and the superscript T denotes the transpose.

The two-branch Eq. (3) predicts that the material behaves like a solid in regions where the stress is below the yield stress ($\tau \leq \tau_0$) and as a fluid in regions where the yield stress is exceeded ($\tau > \tau_0$). These are called unyielded and yielded regions, respectively. It should be noted that unyielded regions include not only regions where the material is stagnant (dead zones) but also zones where the material moves undeformed as a rigid body. The determination of the unyielded and yielded regions, where the two branches of the constitutive equation apply, is a major issue in solving viscoplastic flows. As emphasized by Huilgol [8], this task becomes more difficult in unsteady Bingham flow, since the position and shape of the yielded and unyielded regions has to be determined as a function of space and time. Using regularized versions of the constitutive equation has been a very popular approach in tackling this problem. The main alternative approach is the use of Augmented Lagrangian Methods (ALMs), which are based on the use of variational inequalities. The advantages and disadvatanges of the two approaches are well known and have been recently reviewed by Glowinski and Wachs [9] and by Balmforth et al. [10].

As in [1], instead of the two-branch Eq. (3) we employ the Papanastasiou regularization [11]:

$$\boldsymbol{\tau} = \left\{ \frac{\tau_0[1 - \exp(-m\dot{\gamma})]}{\dot{\gamma}} + \mu \right\} \dot{\boldsymbol{\gamma}} \tag{6}$$

where m is the stress growth exponent. The above model applies everywhere in the flow field (in both yielded and practically unyielded regions) and at the same time provides a satisfactory approximation of the Bingham model for sufficiently large values of the parameter m. This has been tested in numerous benchmark problems [11,12].

The analogy between Eqs. (1) and (3) is obvious. Difficulties analogous to those encountered when using the discontinuous Bingham model also arise when employing the discontinuous slip Eq. (1). Together with the unknown velocity and pressure fields, one has to determine the regions of the wall where slip occurs and those where the no-slip boundary condition applies. Such a task may be trivial to deal with in the case of steady one-dimensional Poiseuille flows but it becomes very difficult in the case of time-dependent two- and three-dimensional flows. Even in the case of Newtonian flows, it is not possible to obtain analytically the parts of the wall where slip occurs. Again, both the regularization and augmented Lagrangian approaches can be used [1,13]. In the present work, we use the following regularization of Eq. (1):

$$\tau_w = \tau_c[1 - \exp(-m_c u_w)] + \beta u_w \tag{7}$$

where m_c is a growth parameter similar to the stress growth exponent m of Eq. (6).

Eq. (7) has been tested by Damianou et al. [14] in solving the cessation of Poiseuille flow of a Herschel-Bulkley fluid in a round tube, which is one dimensional. It has also been used to solve the two-dimensional steady-state Poiseuille flow in a rectangular channel [1], giving very satisfactory results for both Newtonian and Bingham flows in those intermediate regimes where wall slip is partial, i.e. it occurs only along a part of the wall around the symmetry plane. The numerical results also agreed with the analytical solution of the Newtonian flow, in regimes where such a solution is available (no wall slip or slip everywhere along the walls).

An interesting observation in the case of the cessation of viscoplastic Poiseuille flow in a tube with wall slip with zero slip yield stress (i.e. $\tau_c = 0$) is that the velocity becomes and remains uniform before complete cessation [1]. Moreover, the theoretical stopping time may become infinite whereas in the absence of slip this is finite. Damianou et al. [14] employed a power-law generalization of the Navier condition

$$\tau_w = \beta u_w^s \tag{8}$$

and showed that the stopping time is finite only when the exponent s is less than unity; otherwise, the stopping time is infinite for any non-zero Bingham number and the volumetric flow rate decays exponentially. However, if the slip yield stress is non-zero, slip ceases at a finite critical time and cessation is accelerated so that the stopping times are finite, in agreement with theoretical estimates [15,16].

The literature concerning solutions of the steady-state viscoplastic flow in rectangular ducts has been reviewed in [1]. In particular, Roquet and Saramito [13] identified the various steady-state regimes observed when the yield stress and the slip yield stress vary and the slip coefficient is fixed. Time-dependent Bingham flows in ducts of various cross-sections with no wall slip have been studied by Muravleva and Muravleva [17] who considered both start-up and cessation flows. The calculated stopping times for the latter flows were found to be in good agreement with the theoretical estimates.

The objective of the present work is to investigate the effect of wall slip on the cessation flow of a Bingham plastic in a square duct. To our knowledge, this flow has not been investigated before. Moreover, it provides a good test for the regularizations of both the Bingham constitutive equation and the slip equation we employ. The rest of the paper is organized as follows. In Section 2, the governing equations of the flow are presented. In Section 3, we provide analytical solutions for the Newtonian flow in the cases of no wall slip, Navier slip, and slip with nonzero slip yield stress. In the latter case, the flow is amenable to analytical solution only below a first and above a second critical value of the pressure gradient. Below the first critical value, the classical no-slip time-dependent solution applies. Above the second one, non-uniform slip occurs everywhere along the wall and the corresponding analytical solution is valid only until slip at the duct corner ceases and thus slip along the wall is partial (nonlinear) thereafter. In Section 4, we present numerical solutions of the Newtonian flow in all the flow regimes. The numerical results coincide with the analytical ones in all regimes where the latter solutions are available. In Section 5, results for the Bingham flow are presented and the no-slip, Navier-slip, and non-zero-slip-yield-stress cases are discussed. It is shown that when Navier slip applies, i.e. when the slip yield stress is zero, the fluid slips at all times and the velocity becomes and remains flat till complete cessation. The evolution of the flat velocity is solved analytically. Interestingly, numerical difficulties are observed in this flow regime, since the regularization becomes problematic when the rate of deformation is zero almost everywhere (but not very close to the wall). Finally, in Section 6 the main conclusions of this work are summarized.

2. Governing equations

We consider the transient Poiseuille flow of a Bingham plastic in a duct of square cross-section and infinite length with $-H \leq y \leq H$, $-H \leq z \leq H$, where H is the half-width of the duct. Due to symmetry, only the first quadrant is considered. The flow is governed by the momentum equation, which, under the assumption of negligible gravity, is simplified to

$$\rho \frac{\partial u_x}{\partial t} = G + \frac{\partial \tau_{yx}}{\partial y} + \frac{\partial \tau_{zx}}{\partial z} \tag{9}$$

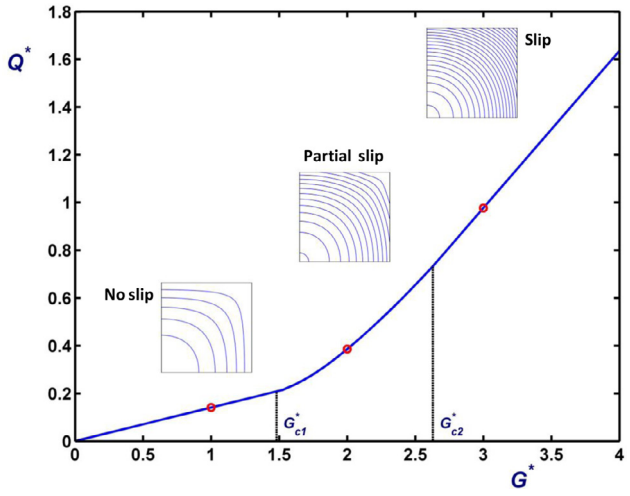

Fig. 1. Flow curve of Newtonian Poiseuille flow in a square duct in the case of non-zero slip yield stress with $B = 1$. Three flow regimes are defined by the two critical values of the imposed pressure gradient ($G^*_{c1} = 1.4808$ and $G^*_{c2} = 2.6290$). The velocity contours for three representative values of the pressure gradient in the three flow regimes ($G^* = 1$, 2, and 3) are also shown.

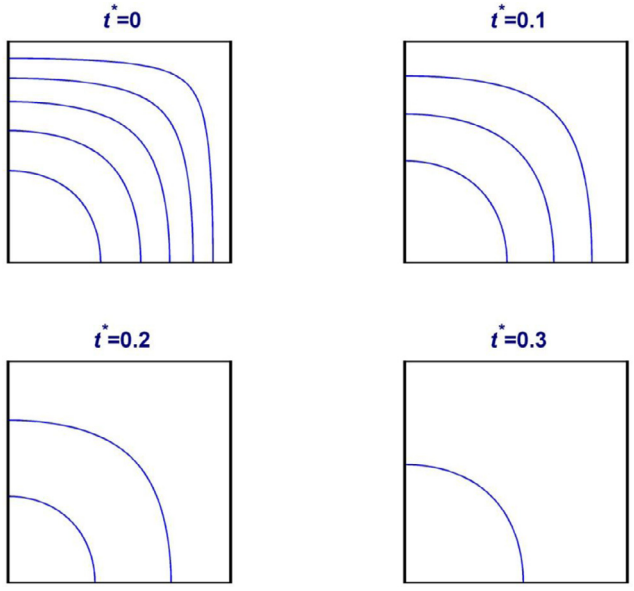

Fig. 2. Evolution of the velocity contours during cessation of Newtonian flow in the case of non-zero slip yield stress with $B = 1$ and $G^* = 1 < G^*_{c1}$ (no wall slip at all times). A step of 0.05 was used for the contour values.

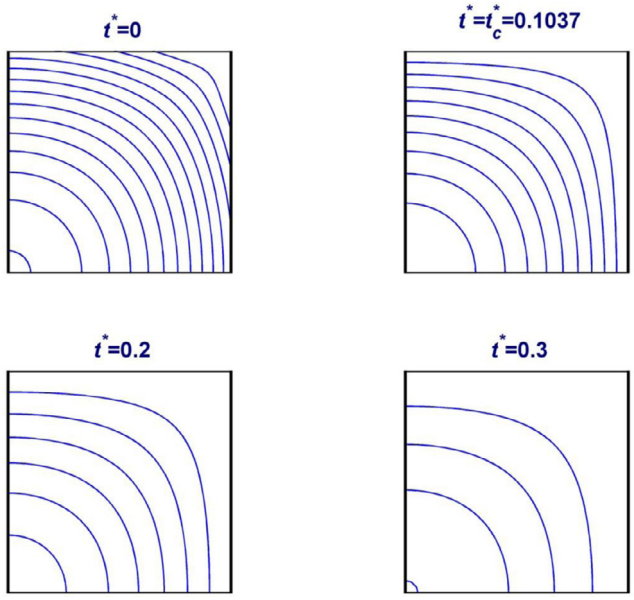

Fig. 3. Evolution of the velocity contours during cessation of Newtonian flow in the case of non-zero slip yield stress with $B = 1$ and $G^*_{c1} < G^* = 2 < G^*_{c2}$ (partial slip at $t^* = 0$). A step of 0.05 was used for the contour values.

where ρ is the density, G is the constant pressure gradient, and τ_{yx} and τ_{zx} are the corresponding components of the viscous stress tensor $\boldsymbol{\tau}$ which is given by the regularized Eq. (6). Along the walls it is assumed that slip occurs following the regularized slip Eq. (7).

To non-dimensionalize the governing equations we scale the velocity and the pressure by appropriate scales, denoted by V_s and P_s, respectively, lengths by H, and the time t by $\rho H^2/\mu$. Hence the flow domain becomes $0 \le y*, z* \le 1$, where the stars denote dimensionless variables. In the case the volumetric flow rate is imposed, the mean velocity V in the duct is used as the velocity scale, i.e. $V_s = V$ and $P_s = \mu V/H$. The non-dimensionalized forms of the momentum and the constitutive equations, given respectively by (9) and (6), are

$$\frac{\partial u_x^*}{\partial t^*} = G^* + \frac{\partial \tau_{yx}^*}{\partial y^*} + \frac{\partial \tau_{zx}^*}{\partial z^*} \tag{10}$$

and

$$\boldsymbol{\tau}^* = \left\{ \frac{Bn[1 - \exp(-M\dot{\gamma}^*)]}{\dot{\gamma}^*} + 1 \right\} \dot{\boldsymbol{\gamma}}^* \tag{11}$$

where

$$Bn \equiv \frac{\tau_0 H}{\mu V} \quad \text{and} \quad M \equiv \frac{mV}{H} \tag{12}$$

are the Bingham number and the dimensionless stress growth number, respectively.

The dimensionless form of the regularized slip Eq. (7) is

$$\tau_w^* = B_c[1 - \exp(-M_c u_w^*)] + Bu_w^* \tag{13}$$

where the slip-yield-stress number, B_c, the slip number, B, and the growth number, M_c, are defined as follows:

$$B_c \equiv \frac{\tau_c H}{\mu V}, \quad B \equiv \frac{\beta H}{\mu}, \quad M_c \equiv m_c V \tag{14}$$

Slip Eq. (7) and its various special cases serves as the boundary condition along the walls while symmetry boundary conditions are employed along the planes of symmetry.

When the pressure gradient is imposed, we take $V_s = H\tau_0/\mu$ and $P_s = \tau_0$. It turns out that the dimensionless governing Eqs. (6)–(8) still apply, the only differences being in the definitions of the following dimensionless numbers:

$$Bn \equiv 1, \quad M \equiv \frac{m\,\tau_0}{H}, \quad B_c \equiv \frac{\tau_c}{\tau_0}, \quad \text{and} \quad M_c \equiv \frac{m_c H \tau_0}{\mu} \tag{15}$$

(The definition of the slip number is the same in both non-dimensionalizations.)

The steady-state Poiseuille flow in a duct has been studied in [1]. In the present work, we consider the cessation of the flow, i.e. at $t^* = 0$ the velocity is given by the steady-state solution and the pressure gradient $G*$ in Eq. (10) is set to zero.

3. Analytical solutions for Newtonian flow

In the case of Newtonian flow in a rectangular duct, Eq. (9) is simplified to

$$\rho \frac{\partial u_x}{\partial t} = G + \eta \left(\frac{\partial^2 u_x}{\partial y^2} + \frac{\partial^2 u_x}{\partial z^2} \right) \tag{16}$$

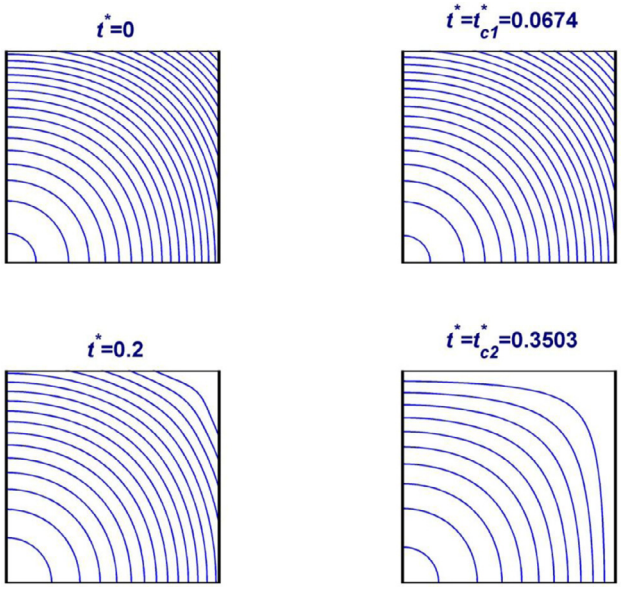

Fig. 4. Evolution of the velocity contours during cessation of Newtonian flow in the case of non-zero slip yield stress with $B = 1$ and $G^* = 3 > G^*_{c2}$ (slip occurs everywhere at $t^* = 0$). A step of 0.05 was used for the contour values.

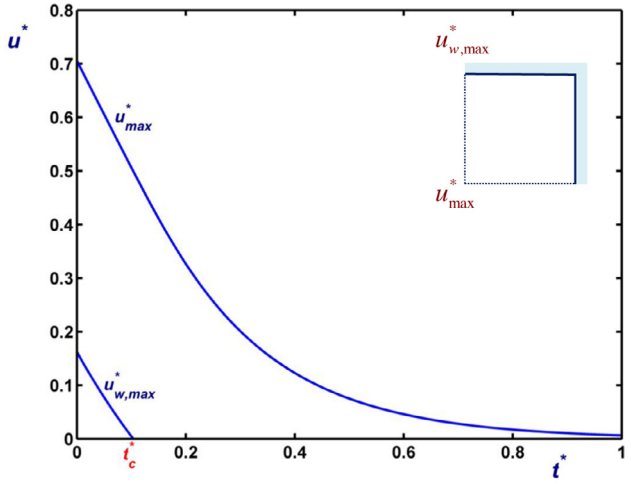

Fig. 5. Evolution of the maximum velocity at the duct center and the maximum slip velocity at the middle of the duct wall during cessation of Newtonian flow in the case of non-zero slip yield stress with $B = 1$ and $G^*_{c1} < G^* = 2 < G^*_{c2}$ (partial slip at $t^* = 0$).

where η is the viscosity. The steady-state solution serves as the initial condition for the cessation flow. The analytical solutions presented below have been obtained using the standard separation of variables method [18].

No wall slip

In the case of no-slip, the steady-state velocity is given by

$$u_x(y,z) = \frac{4GH^2}{\eta}\sum_{i=1}^{\infty}\sum_{j=1}^{\infty}\frac{(-1)^{i+j}}{\alpha_{i,j}^2\alpha_i\alpha_j}\cos(\alpha_i y/H)\cos(\alpha_j z/H) \tag{17}$$

where

$$\alpha_i \equiv (2i-1)\pi/2 \quad \text{and} \quad \alpha_{i,j}^2 \equiv \alpha_i^2 + \alpha_j^2, \quad i,j = 1,2,\cdots \tag{18}$$

The volumetric flow rate over the first quadrant is given by

$$Q = \frac{4GH^4}{\eta}\sum_{i=1}^{\infty}\sum_{j=1}^{\infty}\frac{1}{\alpha_{i,j}^2\alpha_i^2\alpha_j^2} \tag{19}$$

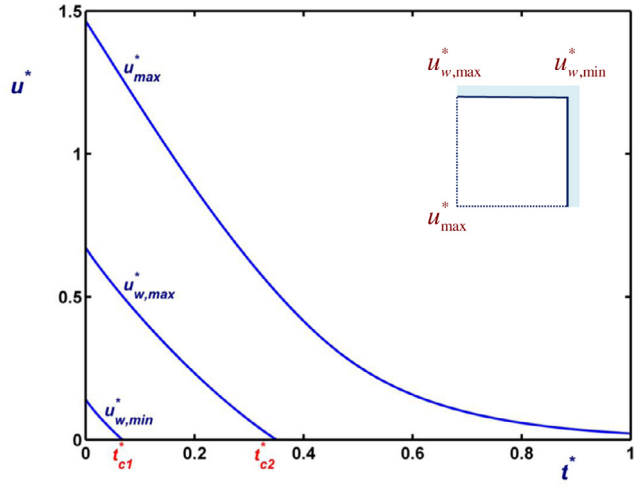

Fig. 6. Evolution of the maximum velocity at the duct center, the maximum slip velocity at the middle of the duct wall, and the minimum velocity at the corner during cessation of Newtonian flow in the case of non-zero slip yield stress with $B = 1$ and $G^* = 3 > G^*_{c2}$ (slip occurs everywhere at $t^* = 0$).

In the transient flow, the pressure gradient is suddenly set to zero and the steady-state solution serves as the initial condition. One then finds that [19]

$$u_x(y,z,t) = \frac{4GH^2}{\eta}\sum_{i=1}^{\infty}\sum_{j=1}^{\infty}\frac{(-1)^{i+j}}{\alpha_{i,j}^2\alpha_i\alpha_j} \times \cos(\alpha_i y/H)\cos\left(\alpha_j z/H\right)\exp(-\alpha_{i,j}^2\nu t/H^2) \tag{20}$$

and

$$Q(t) = \frac{4GH^4}{\eta}\sum_{i=1}^{\infty}\sum_{j=1}^{\infty}\frac{1}{\alpha_{i,j}^2\alpha_i^2\alpha_j^2}\exp(-\alpha_{i,j}^2\nu t/H^2) \tag{21}$$

Navier slip

In the case of Navier slip (zero slip yield stress), non-uniform slip occurs everywhere along the walls for any non-zero value of the pressure gradient. One gets

$$u_x(y,z) = \frac{4GH^2}{\eta}\sum_{i=1}^{\infty}\sum_{j=1}^{\infty}A_{i,j}\frac{1}{\lambda_{i,j}^2}\cos(\lambda_i y/H)\cos(\lambda_j z/H) \tag{22}$$

where

$$\lambda_i\tan\lambda_i = B \quad \text{and} \quad \lambda_{i,j}^2 \equiv \lambda_i^2 + \lambda_j^2, \quad i,j = 1,2,\cdots \tag{23}$$

and

$$B \equiv \frac{\beta H}{\eta} \tag{24}$$

is the slip number. Moreover,

$$A_{i,j} \equiv \frac{\sin(\lambda_i)\sin(\lambda_j)}{\lambda_i\lambda_j(1+\sin^2(\lambda_i)/B)(1+\sin^2(\lambda_j)/B)} \tag{25}$$

Though equivalent, the present representation of the solution is substantially simpler than that used previously by Kaoullas and Georgiou [20]. It should also be noted that the slip number defined in (24) is the inverse of the slip number used in [20]. The volumetric flow rate is given by:

$$Q = \frac{4GH^4}{\eta}\sum_{i=1}^{\infty}\sum_{j=1}^{\infty}A_{i,j}\frac{\sin(\lambda_i)\sin(\lambda_j)}{\lambda_{i,j}^2\lambda_i\lambda_j} \tag{26}$$

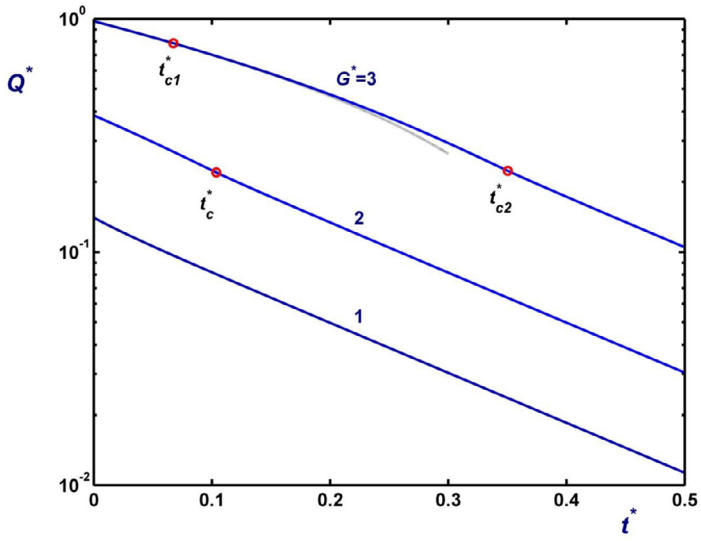

Fig. 7. Evolution of the volumetric flow rate during cessation of Newtonian flow in the case of non-zero slip yield stress with $B = 1$ and various values of the imposed pressure gradient (G^*=1, 2, and 3), which correspond to the three different flow regimes illustrated in Fig. 2. The circles indicate the critical times for a cessation of slip (t^*_c for $G^* = 2$ and t^*_{c1} and t^*_{c2} for $G^* = 3$). The grey lines are the analytical predictions of Eq. (41) which coincide with the numerical ones.

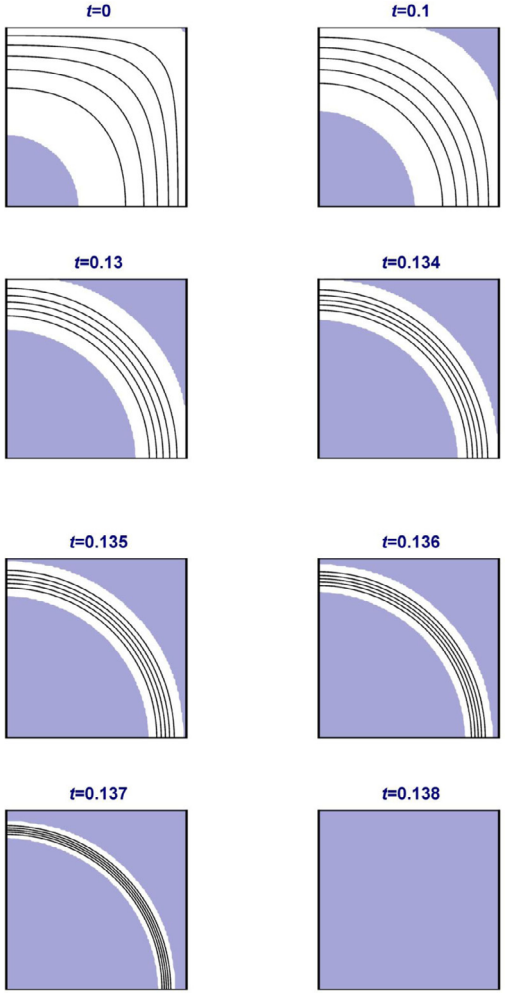

Fig. 8. Unyielded areas (shaded) and velocity contours in cessation of Bingham flow in a square duct ($\alpha = 1$) with no slip at the wall for $\lambda = 0.2$.

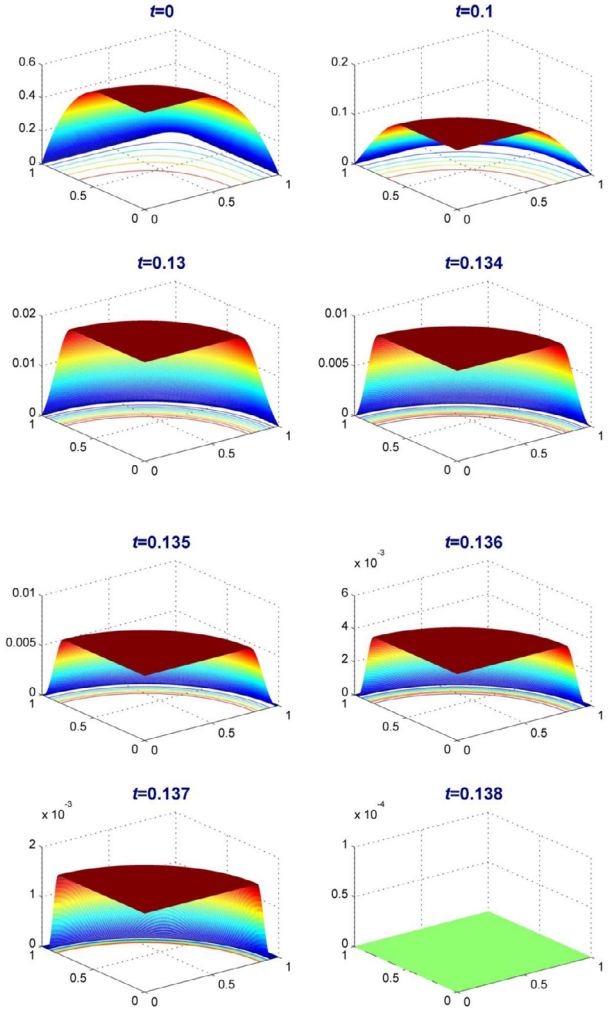

Fig. 9. Evolution of the velocity in cessation of Bingham flow in a square duct ($\alpha = 1$) with no slip at the wall for $\lambda = 0.2$.

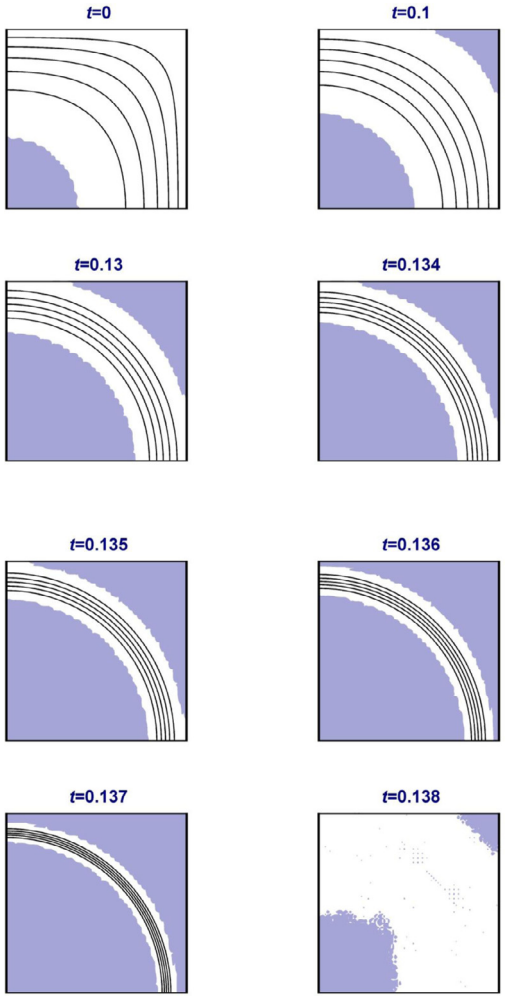

Fig. 10. Unyielded areas (shaded) and velocity contours in cessation of Bingham flow in a square duct with no slip at the wall for $\lambda = 0.2$ obtained with a 40×40-element mesh.

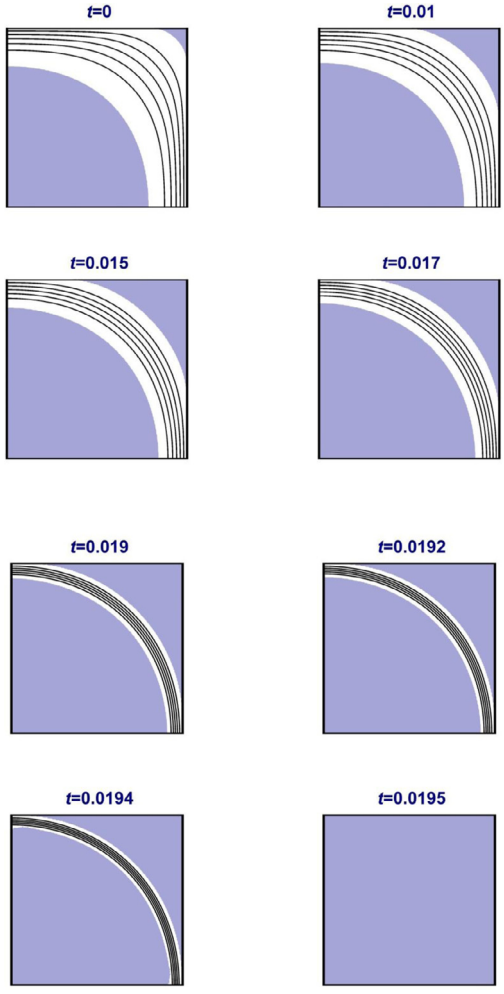

Fig. 11. Unyielded areas (shaded) and velocity contours in cessation of Bingham flow in a square duct with no slip at the wall for $\lambda = 0.4$.

The velocity and the volumetric flow rate in the case of cessation are

$$u_x(y,z,t) = \frac{4GH^2}{\eta}\sum_{i=1}^{\infty}\sum_{j=1}^{\infty}A_{i,j}\frac{1}{\lambda_{i,j}^2}\cos(\lambda_i y/H)\cos\left(\lambda_j z/H\right) \times \exp(-\lambda_{i,j}^2 \nu t/H^2) \tag{27}$$

and

$$Q(t) = \frac{4GH^4}{\eta}\sum_{i=1}^{\infty}\sum_{j=1}^{\infty}A_{i,j}\frac{\sin(\lambda_i)\sin\left(\lambda_j\right)}{\lambda_{i,j}^2\lambda_i\lambda_j}\exp(-\lambda_{i,j}^2\nu t/H^2) \tag{28}$$

Slip with non-zero slip yield stress

In the case of non-zero slip yield stress, there is no wall slip below the critical pressure gradient G_{c1} at which the wall shear stress at the middle of the duct wall is equal to τ_c. From Eq. (17) we find that the steady-state wall shear stress along the wall $y = H$ is

$$\tau_w(z) = 4GH\sum_{i=1}^{\infty}\sum_{j=1}^{\infty}\frac{(-1)^{j+1}\cos(\alpha_j z/H)}{\alpha_{i,j}^2\alpha_j} \tag{29}$$

For $G = G_{c1}$ we have $\tau_w(0) = \tau_c$. Hence

$$G_{c1} = \frac{\tau_c}{4H\sum_{i=1}^{\infty}\sum_{j=1}^{\infty}\frac{(-1)^{j+1}}{\alpha_{i,j}^2\alpha_j}} \tag{30}$$

The second critical value of the pressure gradient, G_{c2}, above which non-uniform slip occurs everywhere is found to be given by:

$$G_{c2} = \frac{\tau_c}{4H\sum_{i=1}^{\infty}\sum_{j=1}^{\infty}\frac{A_{i,j}\lambda_i\sin\lambda_i\cos\lambda_j}{\lambda_{i,j}^2}} \tag{31}$$

The two critical values of the pressure gradient define three flow regimes as follows: (i) for $G \le G_{c1}$, no slip occurs and the velocity and volumetric flow rates are given by the no-slip solution, i.e. by Eqs. (17) and (19); (ii) for $G_{c1} < G \le G_{c2}$, slip occurs in the middle of the edges but not near the corners and the problem is not amenable to analytical solution; (iii) for $G > G_{c2}$, non-uniform slip occurs everywhere and the velocity and the volumetric flow rate are given respectively by

$$u_x(y,z) = \frac{4GH^2}{\eta}\sum_{i=1}^{\infty}\sum_{j=1}^{\infty}A_{i,j}\frac{1}{\lambda_{i,j}^2}\cos(\lambda_i y/H)\cos\left(\lambda_j z/H\right) - \frac{\tau_c H}{\eta B} \tag{32}$$

and

$$Q = \frac{4GH^4}{\eta}\sum_{i=1}^{\infty}\sum_{j=1}^{\infty}A_{i,j}\frac{\sin(\lambda_i)\sin\left(\lambda_j\right)}{\lambda_{i,j}^2\lambda_i\lambda_j} - \frac{4\tau_c H^3}{\eta B} \tag{33}$$

where $A_{i,j}$ and λ_i have already been defined in the Navier-slip case.

The form of the time-dependent solution changes depending on the regime of the steady-state. If $G \le G_{c1}$, then the time-dependent

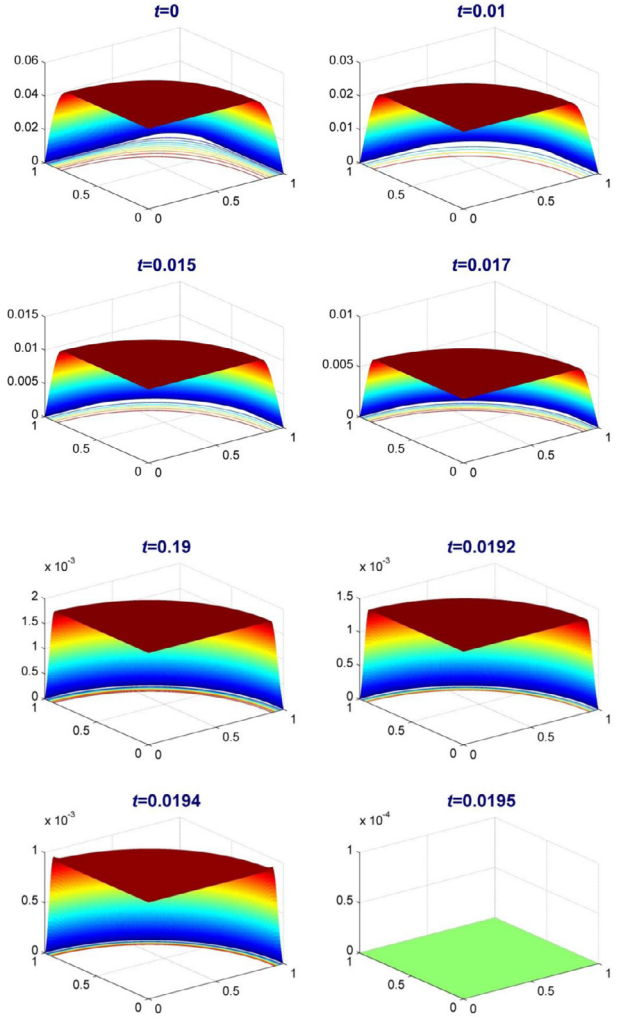

Fig. 12. Evolution of the velocity in cessation of Bingham flow in a square duct ($\alpha = 1$) with no slip at the wall for $\lambda = 0.4$.

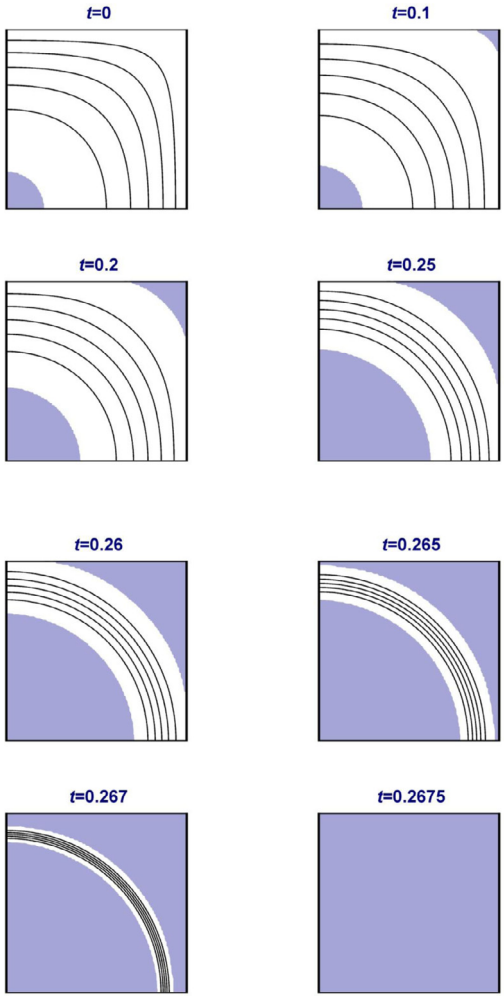

Fig. 13. Unyielded areas (shaded) and velocity contours in cessation of Bingham flow in a square duct with no slip at the wall for $Bn = 1$.

solution is given simply by Eqs. (20) and (21). If $G > G_{c2}$, we have

$$u_x(y,z,t) = \frac{4GH^2}{\eta}\sum_{i=1}^{\infty}\sum_{j=1}^{\infty}A_{i,j}\frac{1}{\lambda_{i,j}^2}\cos(\lambda_i y/H) \times \cos(\lambda_j z/H)\exp(-\lambda_{i,j}^2 \nu t/H^2) - \frac{\tau_c H}{\eta B} \tag{34}$$

and

$$Q(t) = \frac{4GH^4}{\eta}\sum_{i=1}^{\infty}\sum_{j=1}^{\infty}A_{i,j}\frac{\sin(\lambda_i)\sin(\lambda_j)}{\lambda_{i,j}^2\lambda_i\lambda_j}\exp(-\lambda_{i,j}^2\nu t/H^2) - \frac{\tau_c H^3}{\eta B} \tag{35}$$

The above solution holds only till a critical time,t_c, at which the velocity at the duct corners becomes zero. After this time, the flow cannot be solved analytically. This critical time can be found by solving the equation

$$\sum_{i=1}^{\infty}\sum_{j=1}^{\infty}A_{i,j}\frac{1}{\lambda_{i,j}^2}\cos\lambda_i\cos\lambda_j\exp(-\lambda_{i,j}^2\nu t_c/H^2) = \frac{\tau_c}{4HBG} \tag{36}$$

Non-dimensionalization

For the flow with non-zero slip yield stress, we use a different set of scales, i.e. we scale the velocity by $H\tau_c/\eta$, the pressure gradient by τ_c/H, y and z by H, and time by H^2/ν. The non-dimensionalized values of the critical pressure gradients are

$$G_{c1}^* = \frac{1}{4\sum_{i=1}^{\infty}\sum_{j=1}^{\infty}\frac{(-1)^{j+1}}{\alpha_{i,j}^2\alpha_j}} \tag{37}$$

and

$$G_{c2}^* = \frac{1}{4\sum_{i=1}^{\infty}\sum_{j=1}^{\infty}\frac{A_{i,j}\lambda_i\sin\lambda_i\cos\lambda_j}{\lambda_{i,j}^2}} \tag{38}$$

The velocity and volumetric flow rate can be written as follows:

$$u_x^*(y^*,z^*,t^*) = \begin{cases} 4G^*\sum_{i=1}^{\infty}\sum_{j=1}^{\infty}\frac{(-1)^{i+j}}{\alpha_{i,j}^2\alpha_i\alpha_j}\cos(\alpha_i y^*)\cos(\alpha_j z^*)\exp(-\alpha_{i,j}^2 t^*), & G^* \le G_{c1}^* \\ 4G^*\sum_{i=1}^{\infty}\sum_{j=1}^{\infty}A_{i,j}\frac{1}{\lambda_{i,j}^2}\cos(\lambda_i y^*)\cos(\lambda_j z^*)\exp(-\lambda_{i,j}^2 t^*) - \frac{1}{B}, & G^* \ge G_{c2}^* \end{cases} \tag{39}$$

and

$$Q^*(t^*) = \begin{cases} 4G^*\sum_{i=1}^{\infty}\sum_{j=1}^{\infty}\frac{1}{\alpha_{i,j}^2\alpha_i^2\alpha_j^2}\exp(-\alpha_{i,j}^2 t^*) & G^* \le G_{c1}^* \\ 4G^*\sum_{i=1}^{\infty}\sum_{j=1}^{\infty}A_{i,j}\frac{\sin(\lambda_i)\sin(\lambda_j)}{\lambda_{i,j}^2\lambda_i\lambda_j}\exp(-\lambda_{i,j}^2 t^*) - \frac{1}{B}, & G^* \ge G_{c2}^* \end{cases} \tag{40}$$

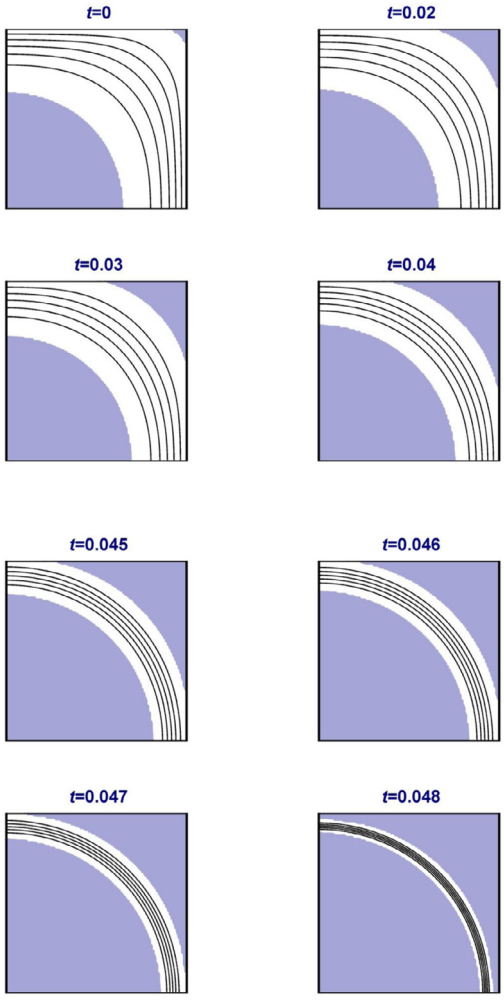

Fig. 14. Unyielded areas (shaded) and velocity contours in cessation of Bingham flow in a square duct with no slip at the wall for $Bn = 10$.

In the above two expressions, the solution for $G^* \le G^*_{c1}$ holds at all times, while the solution for $G^* > G^*_{c2}$ holds only till the critical time t^*_c at which slip at the duct corner ceases. The time t^*_c is the root of the following equation:

$$\sum_{i=1}^{\infty}\sum_{j=1}^{\infty} A_{i,j}\frac{1}{\lambda^2_{i,j}}\cos\lambda_i\cos\lambda_j\exp(-\lambda^2_{i,j}t^*_c) = \frac{1}{4BG^*} \tag{41}$$

4. Numerical results on cessation of Newtonian flow

In this section, we present numerical results for the Newtonian flow when the slip yield stress is non-zero. Hence, all variables are non-dimensionalized with the scales of Section 3. The finite element method with biquadratic elements for the velocity has been implemented and an 100×100-element mesh has been employed for solving the flow in the first quadrant (thus taking the symmetries of the problem into account). For all the transient Newtonian simulations in this section, the fully-implicit Euler method with a constant timestep $\Delta t^* = 0.0001$ has been used.

The steady-state flow curve, i.e. the plot of the volumetric flow rate versus the imposed pressure gradient, for $B = 1$ is shown in Fig. 1. Three flow regimes are defined by the two critical values $G^*_{c1} = 1.4808$ and $G^*_{c2} = 2.6290$: (a) for $G^* \le G^*_{c1}$, there is no slip along the duct walls; (b) for $G^*_{c1} < G^* \le G^*_{c2}$ slip is partial, i.e. it occurs in the middle of each edge and not close the corners; and (c) for $G^* > G^*_{c2}$ slip occurs everywhere along the boundary. The velocity contours for three representative values of the pressure gradient, i.e. G^*=1, 2, and 3, corresponding to the three regimes are also illustrated in Fig. 1.

The evolution of the velocity contours in the case of cessation for the three selected values of the pressure gradient (G^*=1, 2, and 3) is illustrated in Figs. 2–4. When G^*=1 (Fig. 2), there is no wall slip at all times. When G^*=2 (Fig. 3), partial slip is observed only initially. As the velocity is reduced under the influence of viscosity, wall slip eventually ceases at a critical time $t^*_c = 0.1037$ after which the velocity vanishes in a fashion similar to that of the no-slip case. In this work it is assumed that slip at a given wall point ceases when the velocity becomes less than the 10^{-4} tolerance used in our simulations. Fig. 5 shows the evolution of the maximum velocity value at the duct center, $u^*_{\max}$, and that of the maximum slip velocity at the middle of the duct edges, $u^*_{w,\max}$. It is clear that the former decays fast initially and then goes exponentially to zero, whereas the latter decays fast and becomes zero at a finite time, t^*_c.

When $G^* = 3$ (Fig. 4), slip occurs everywhere along the walls initially till the critical time $t^*_{c1} = 0.0674$ at which the slip velocity at the corners becomes zero. In this initial regime the numerical solution coincides with the analytical one and the computed value of t^*_{c1} is indeed the root of Eq. (40). After that time, slip at the wall is

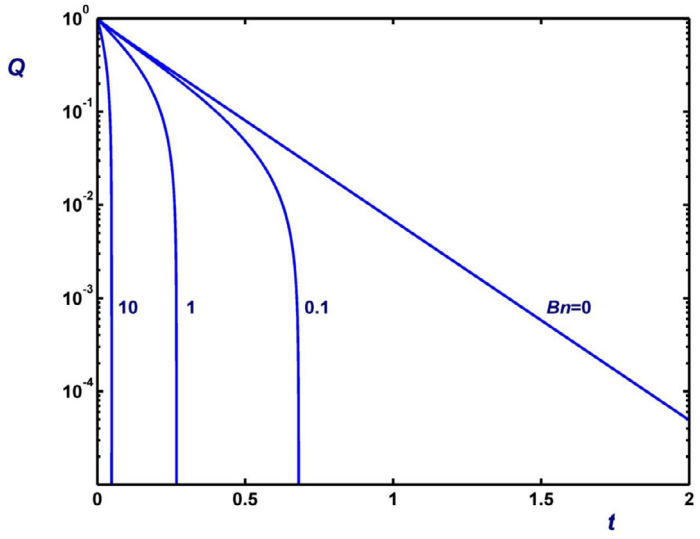

Fig. 15. Evolution of the volumetric flow rates in cessation of Bingham flow in a square duct with no slip at the wall for various Bingham numbers.

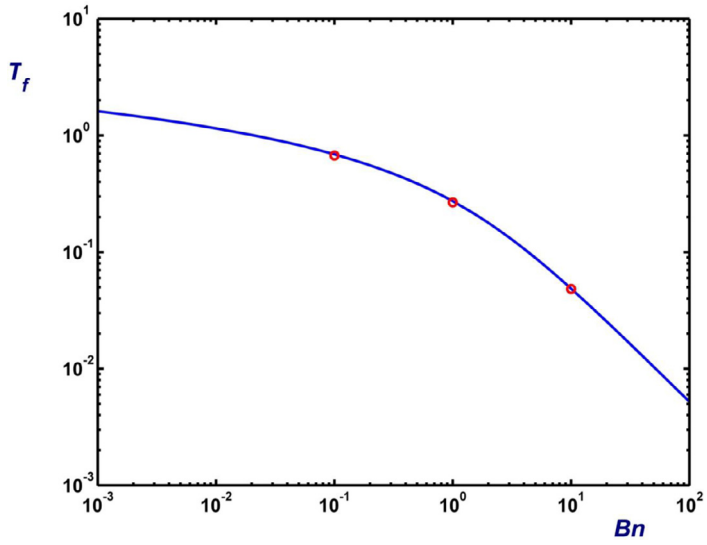

Fig. 16. Theoretical upper bound for the stopping time in cessation of Poiseuille flow in a square duct. The circles correspond to the numerical stopping times.

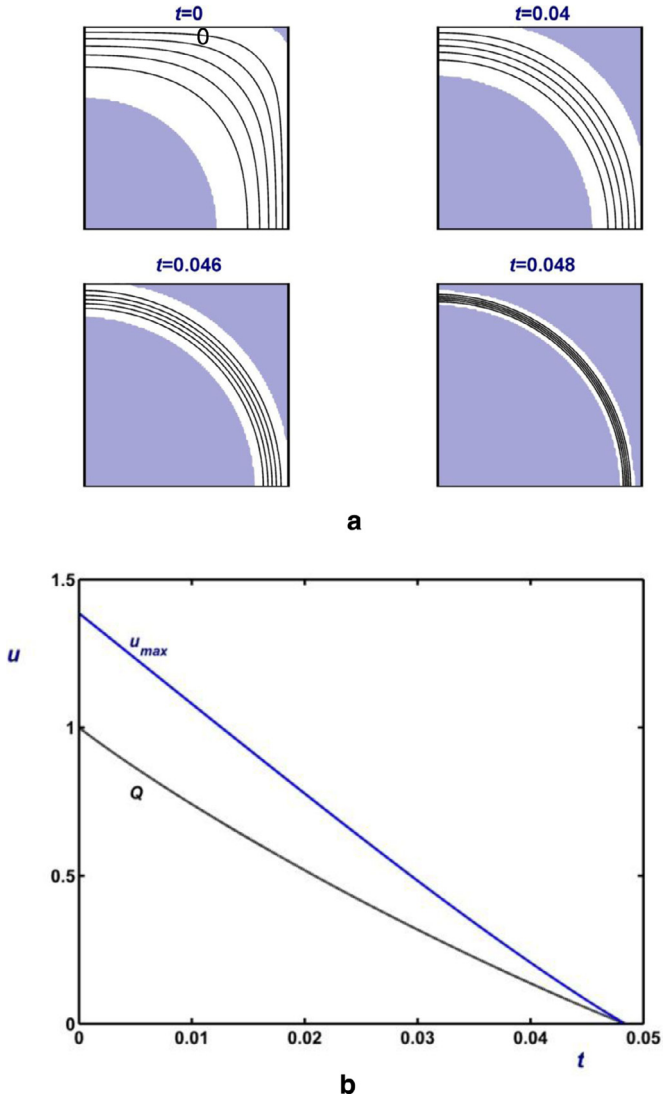

Fig. 17. Cessation of Bingham flow in a square duct with no wall slip for $Bn = 10$: (a) Unyielded areas (shaded) and velocity contours; (b) Evolution of the volumetric flow rate (Q) and the maximum velocity at the duct center (u_{max}).

partial till the critical time $t^*_{c2} = 0.3503$ at which slip ceases. In Fig. 6, we plotted the evolution of the maximum velocity (u^*_{max}), the maximum slip velocity at the middle of the edges ($u^*_{w,max}$), and the minimum slip velocity at the corners ($u^*_{w,min}$). Obviously, $u^*_{w,min}$ and $u^*_{w,max}$ vanish at t^*_{c1} and t^*_{c2}, respectively.

The numerical volumetric flow rates for all the cases we considered here ($G^* = 1$, 2, and 3) are plotted in Fig. 7 along with their analytical counterparts for $G^* = 1$ and 3. The agreement with the analytical results is excellent. Even though the analytical solution for G^*=3 holds only up to t^*_{c1}, we have chosen to plot it outside the full-slip regime in order to make the comparison easier. Once slip ceases ($t* \geq 0$when $G^* = 1$, $t^* \geq t^*_c$when $G^* = 2$, and $t^* \geq t^*_{c2}$when $G^* = 3$) the volumetric flow rate decays exponentially at the same rate. When slip occurs everywhere along the wall (e.g. for $G^* = 3$ and $t^* < t^*_{c1}$) the decay of the volumetric flow rate is slower. It is interesting to note that in the case of partial slip (e.g. for $G^* = 2$ and $t^* < t^*_c$ or for $G^* = 3$ and just before t^*_{c2}) the decay is slightly faster than after the cessation of wall slip. The bending of the curve is due to the constant term that appears in the expression of the volumetric flow rate in Eq. (40).

5. Numerical results on cessation of Bingham plastic flow

The finite element method with biquadratic basis functions for the velocity was used for solving the nonlinear governing equation and the convergence tolerance was set to 10^{-4}. In order to determine accurately the yielded and unyielded regions with a regularization method, one needs to employ fine meshes and a rather high value of the regularization parameter. This was also emphasized in our previous work on the steady-state flow [1]. The "unyielded" areas have been determined as the areas where $\tau* \leq Bn$ (von Mises criterion). Unless otherwise indicated, we used a 100×100-element mesh with $M = 10^6$ to obtain the results of this section. Using such a high value of M is necessary in order to accurately determine the unyielded regions but also to obtain good estimates of the stopping times.

In general, time-dependent Bingham flows require smaller time-steps than their Newtonian counterparts. In the beginning of the cessation flow, we found it necessary to reduce the time step down to 0.001 times its nominal value $\Delta t*$ and gradually increase it up to its nominal value at $t^* = \Delta t^*$. Another observation we made was that coarser meshes require even smaller time steps in order to avoid divergence. Unless otherwise indicated, for the Bingham plastic simulations we used $\Delta t^* = 0.00001$, a rather low value, which was partially dictated by the use of a fine mesh and the huge value for M. The convergence of the results has been checked by means of comparisons to

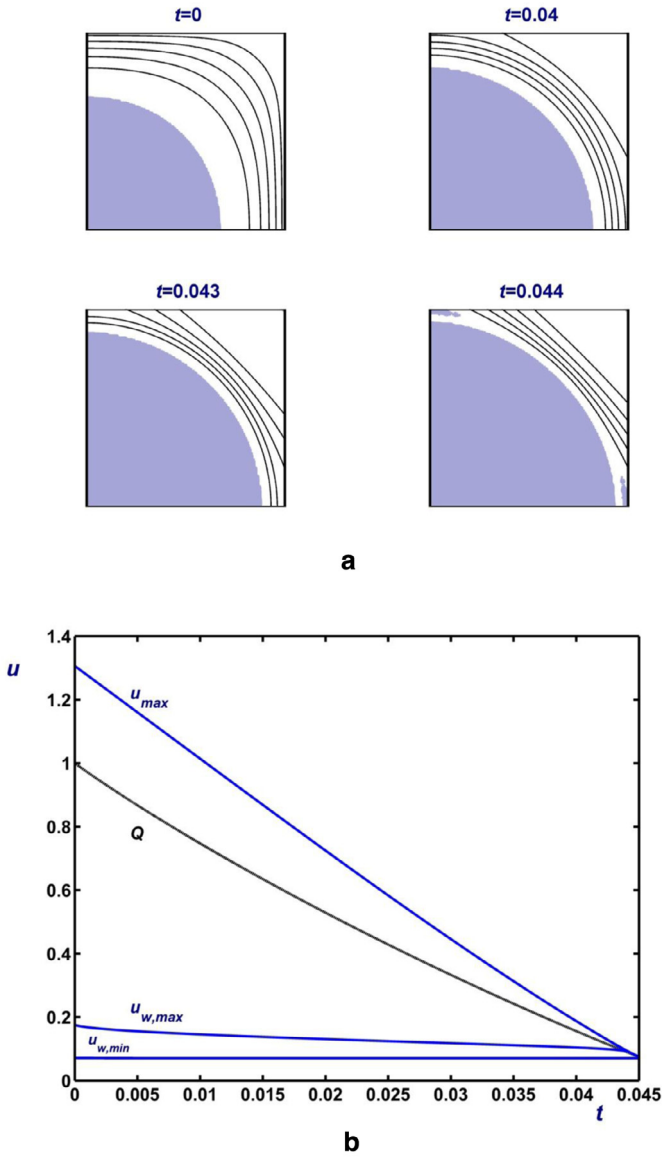

Fig. 18. Cessation of Bingham flow in a square duct with wall slip for $Bn = 10$ and $B = 100$: (a) Unyielded areas (shaded) and velocity contours; (b) Evolution of the volumetric flow rate (Q), the maximum velocity at the duct center ($u_{\max}$), the maximum slip velocity at the middle of the duct wall ($u_{w,\max}$), and the minimum slip velocity at the duct corner ($u_{w,\min}$).

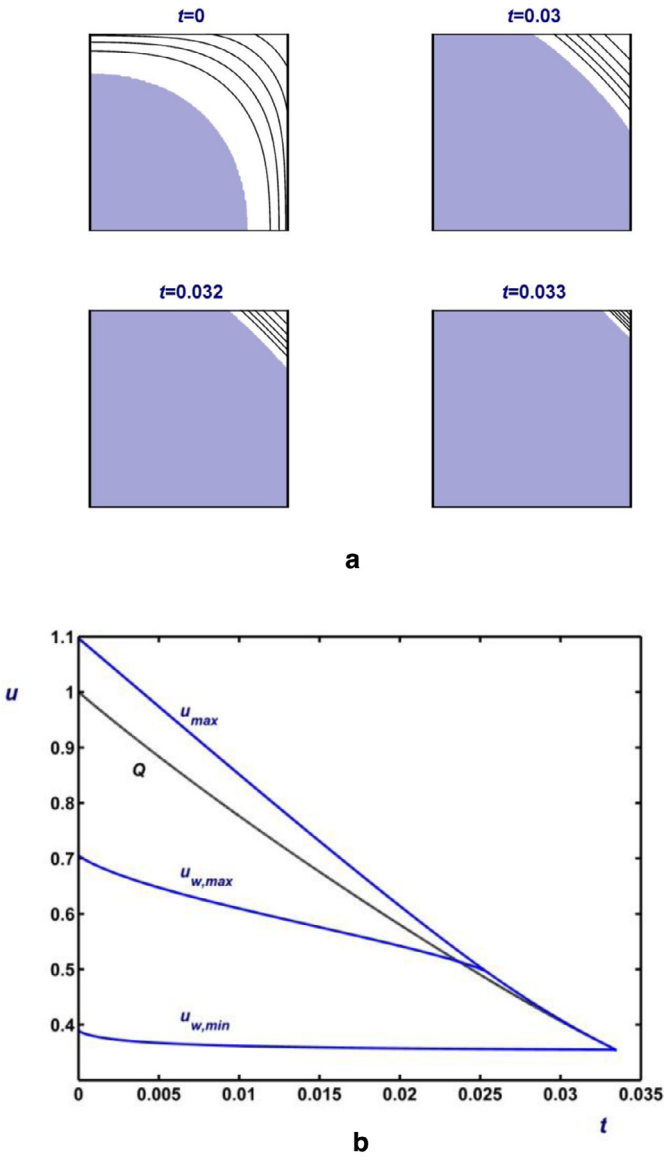

Fig. 19. Cessation of Bingham flow in a square duct with wall slip for $Bn = 10$ and $B = 20$: (a) Unyielded areas (shaded) and velocity contours; (b) Evolution of the volumetric flow rate (Q), the maximum velocity at the duct center ($u_{\max}$), the maximum slip velocity at the middle of the duct wall ($u_{w,\max}$), and the minimum slip velocity at the duct corner ($u_{w,\min}$).

solutions obtained with smaller and/or bigger time steps in several cases. For simplicity, the stars denoting dimensionless variables will be dropped hereafter.

5.1. No wall slip

We first obtained results with the initial condition corresponding to a given fixed pressure gradient which is suddenly set to zero. More specifically, results have been obtained for different values of the parameter

$$\lambda \equiv \frac{1}{G} \tag{42}$$

In Fig. 8, we show the evolution of the velocity and of the yielded/unyielded regions for $\lambda = 0.2$. We can observe how the plug core and the stagnant corner regions increase in size and eventually merge causing the flow to stop. Due to the no-slip boundary condition the merging curve always lies inside the duct. This has also been observed by Muravleva and Muravleva [17] who noted that the stagnant regions just before cessation surround the entire boundary contour. Fig. 9 shows the 3D graph of the velocity (note that the y-axis scales are reduced considerably just before cessation). To demonstrate the importance of mesh refinement, we show in Fig. 10 the results obtained with a 40×40-element mesh. While the velocity is essentially the same, the calculated unyielded regions are not smooth.

Figs. 11 and 12 show the evolution of the solution when $\lambda = 0.4$. Given that increasing λ is equivalent to reducing the imposed pressure gradient, the flow ceases much faster in this case.

Results have also been obtained when the volumetric rate is imposed initially ($Q = 1$) and the corresponding pressure gradient (which depends on the Bingham number) is suddenly set to zero. The results for Bn=1 and 10 are presented in Figs. 13 and 14, respectively. One observes that the merging curve of the unyielded regions moves towards the walls as the Bingham number is increased, in agreement with the calculations of Muravleva and Muravleva [17]. Obviously, the stopping time is reduced as the Bingham number is increased. This is more clearly seen in Fig. 15 where we plot the evolution of the

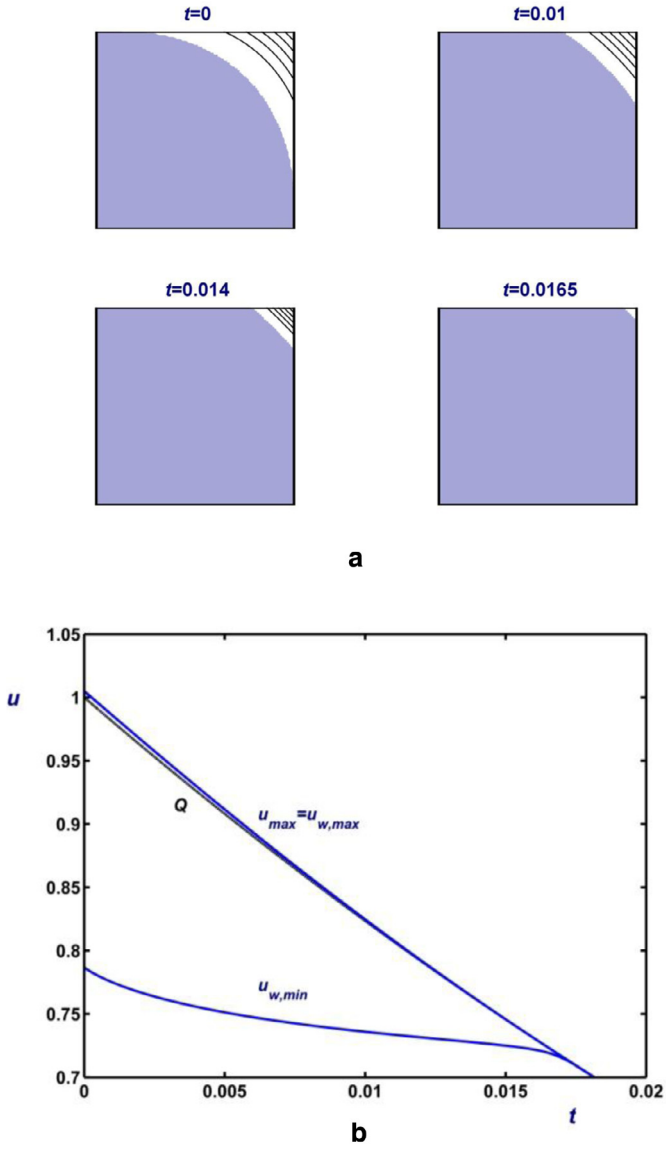

Fig. 20. Cessation of Bingham flow in a square duct with wall slip for $Bn = B = 10$: (a) Unyielded areas (shaded) and velocity contours; (b) Evolution of the volumetric flow rate (Q), the maximum velocity at the duct center (u_{max}), the maximum slip velocity at the middle of the duct wall ($u_{w,max}$), and the minimum slip velocity at the duct corner ($u_{w,min}$).

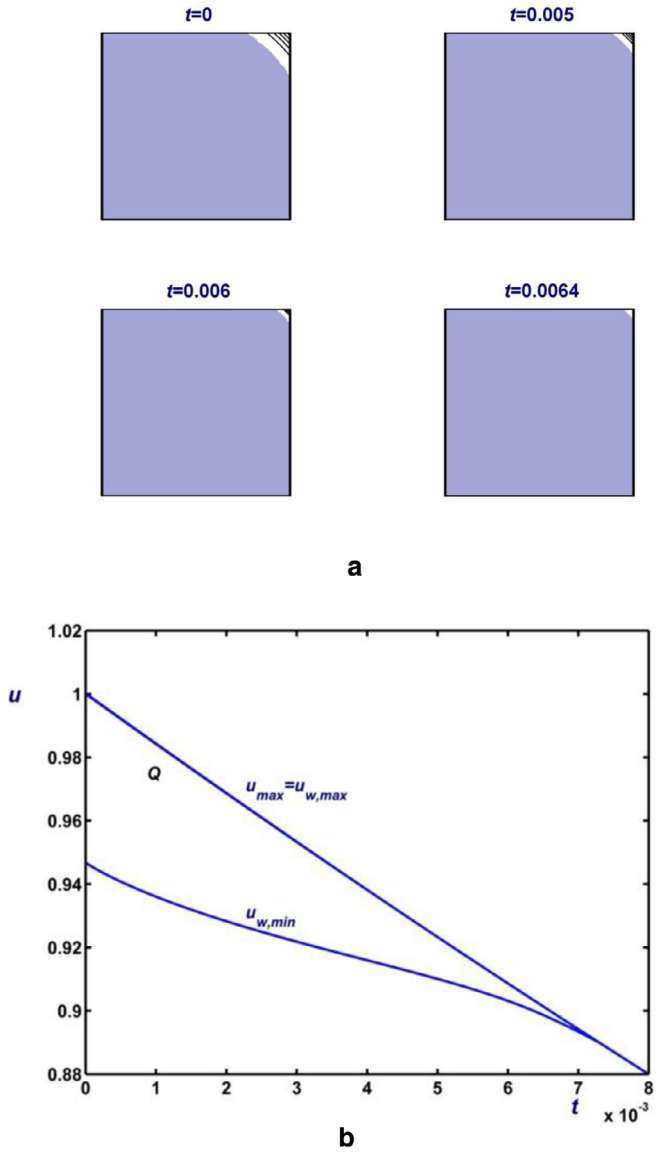

Fig. 21. Cessation of Bingham flow in a square duct with wall slip for $Bn = 10$ and $B = 8$: (a) Unyielded areas (shaded) and velocity contours; (b) Evolution of the volumetric flow rate (Q), the maximum velocity at the duct center (u_{max}), the maximum slip velocity at the middle of the duct wall ($u_{w,max}$), and the minimum slip velocity at the duct corner ($u_{w,min}$).

volumetric flow rates for $Bn = 0$, 0.1, 1, and 10. The numerical stopping times, i.e. the times at which Q becomes 10^{-3} were found to be equal to 0.674, 0.267 and 0.0483 for $Bn = 0.1$, 1, and 10, respectively.

It should be noted that using a very refined mesh may lead to convergence difficulties in the final stages of cessation, i.e. when the velocity is close to zero and thus flat. In such a case the magnitude of the rate-of-strain tensor is almost zero and thus the use of the regularized constitutive equation becomes problematic. It seems that the main advantage of using a very fine mesh is the possibility of drawing more accurate and smoother yielded regions for times very close to complete cessation. But if convergence becomes difficult then the only other option is to reduce M, which again leads to inaccurate unyielded regions.

The upper bound of Glowinski [15] for the cessation of Poiseuille flow of a Bingham fluid is given by

$$T_f \leq \frac{1}{\alpha_{1,1}^2} \ln\left[1 + \frac{\alpha_{1,1}^2}{2Bn}\|u_x(y,z,0)\|\right] \tag{43}$$

where $u_x(y,z,0)$ is the initial velocity, i.e. the steady-state solution for a given Bn and

$$\|u_x(y,z,0)\| \equiv \left[\int_0^1 \int_0^1 u_x^2(y,z,0)dydz\right]^{1/2} \tag{44}$$

Since $\alpha_{1,1}^2 = \pi^2/2$, one gets

$$T_f \leq \frac{2}{\pi^2} \ln\left[1 + \frac{\pi^2}{4Bn}\|u_x(y,z,0)\|\right] \tag{45}$$

The above upper bound is plotted as function of the Bingham number in Fig. 16, where the numerical stopping times for $Bn = 0.1$, 1, and 10 are also shown. These compare very well with the theory. The dependence of the stopping time upper bound on the density and the plastic viscosity, noted by Muravleva and Muravleva [17], is included in the time scaling we used ($\rho H^2/\mu$) and in the definition of the Bingham number. Therefore, it is not necessary to investigate separately the effects of these two material parameters.

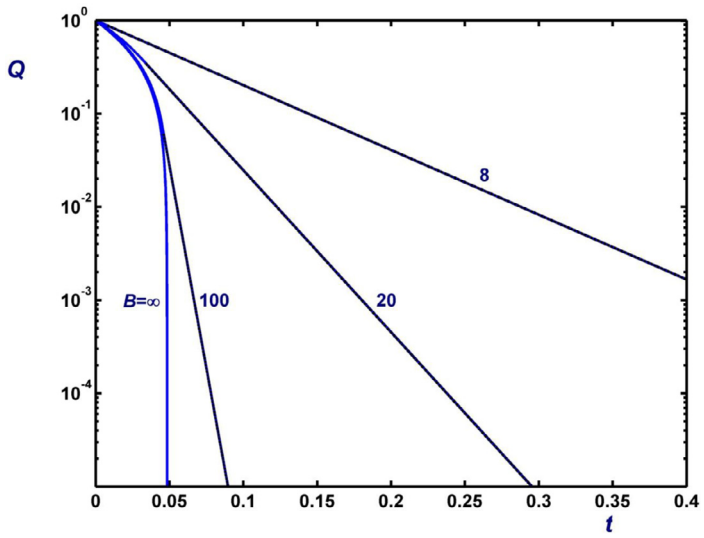

Fig. 22. Evolution of the volumetric flow rate in cessation of Bingham flow in a square duct for $Bn = 10$ and various slip numbers. The predictions of Eq. (50) once the velocity becomes plug, plotted with dashed lines, are indistinguishable from their numerical counterparts.

5.2. Navier slip

In order to visualize the combined effects of slip and viscoplasticity during cessation, we consider once again the evolution of the maximum velocity at the duct center ($u_{\max}$), the maximum slip velocity at the middle of the wall ($u_{w,\max}$), and the minimum slip velocity at the duct corner ($u_{w,\min}$). Obviously, in the absence of slip, $u_{w,\max} = u_{w,\min} = 0$. Moreover, if the growing inner unyielded core reaches the wall, then $u_{w,\max} = u_{\max}$ and if $u_{w,\min} = u_{\max}$, then the velocity is plug.

When the Navier-slip boundary condition is applied, the slip number B in Newtonian flow can take any value from zero (full slip) to infinity (no-slip). In Bingham plastic flow, however, full-slip (i.e. plug flow) is attained at a finite value of B, which turns out to be $B_{crit} = Bn/\sqrt{2}$ for a square duct [1]. The evolution of the above quantities along with the unyielded regions and velocity contours for Bn=10 and various slip numbers in the range (B_{crit}, ∞) is illustrated in Figs. 17–21. Fig. 17 shows results for the no-slip case ($B = \infty$). The maximum and minimum slip velocities are of course zero and, as expected, $u_{\max}$ is always higher than Q; the two curves intersect only when the flow ceases, i.e., when both quantities vanish.

The results of Fig. 18 for $B = 100$ correspond to weak slip. It is observed that the fluid decelerates faster at the duct center and much slower at the duct corner. In fact, $u_{w,\min}$ appears to remain constant initially. Eventually, all the curves in Fig. 18b merge at a finite time, and the velocity becomes flat before it becomes zero. Our numerical experiments showed that the regularization method we used encounters severe difficulties once the velocity is almost plug, given that the magnitude of the rate-of-strain tensor is zero. The small "unyielded islands" of Fig. 18a at $t = 0.044$ are numerical artifacts due to this phenomenon. As one can deduce from Fig. 18b, the velocity at this time is almost plug and the fluid is essentially unyielded in the entire domain. The results of Fig. 19 for $B = 20$ correspond to stronger slip. As the fluid decelerates, the central plug region grows and reaches the wall. As a result, the curves of $u_{w,\max}$ and $u_{\max}$ merge. The minimum slip velocity $u_{w,\min}$ initially decays slowly and then remains practically constant till the velocity becomes plug. Once it touches the wall, the plug zone continues growing towards the corner and the yielded region attains the shape of a right equilateral triangle while the velocity contours are straight lines. Similar observations are made in Figs. 20 and 21, where slip is much stronger and the velocity is plug except near the duct corners.

As mentioned above, when the velocity becomes almost plug the regularization method starts failing. However, the flow can easily be solved analytically. In the final stage of cessation the velocity is flat and thus equal to the slip velocity $u_w(t)$. Obviously the wall shear stress is everywhere the same, i.e.

$$\tau_w(t) \equiv B u_w(t) \tag{46}$$

In this sliding regime one can assume that the shear stresses τ_{yx} and τ_{zx}vary linearly with y and z, respectively. Hence,

$$\tau_{yx} = -\tau_w(t) y \quad \text{and} \quad \tau_{zx} = -\tau_w(t) z \tag{47}$$

From the momentum equation we get

$$\frac{du_w}{dt} = \frac{\partial \tau_{yx}}{\partial y} + \frac{\partial \tau_{zx}}{\partial z} = -2\tau_w(t) \tag{48}$$

Combining (45) and (47) leads to

$$\frac{du_w}{dt} = -2B u_w(t) \tag{49}$$

the solution of which is

$$u_w(t) = u_{w0} \exp\left[-2B(t - t_0)\right], \quad t \geq t_0 \tag{50}$$

where $t_0$denotes the critical time at which the velocity becomes uniform and $u_{w0} = u_w(t_0)$. It is clear that the flow decays exponentially, i.e. it ceases at infinite time, unlike its no-slip counterpart. The same result was obtained by Damianou et al. [14] for the axisymmetric Poiseuille flow. It was also shown that in the case of a power-law-type slip equation with a power exponent s, the stopping time is finite only is $s<1$. Hence, if

$$\tau_w \equiv B u_w^s \tag{51}$$

(note that the definition of B is different) one finds that for $s \neq 1$

$$u_w(t) = \left[u_{w0}^{1-s} - 2(1-s)B(t - t_0)\right]^{1/(1-s)}, \quad t \geq t_0 \tag{52}$$

Hence, the stopping time is finite only if $s<1$, in which case

$$t_s = t_0 + \frac{u_{w0}^{1-s}}{2(1-s)B} \tag{53}$$

The evolution of the volumetric flow rate is shown in Fig. 22 for different slip numbers. Once the flow becomes plug, Q decays exponentially following Eq. (49). The predictions of the latter equation are also plotted in Fig. 22 and coincide with the numerical solutions.

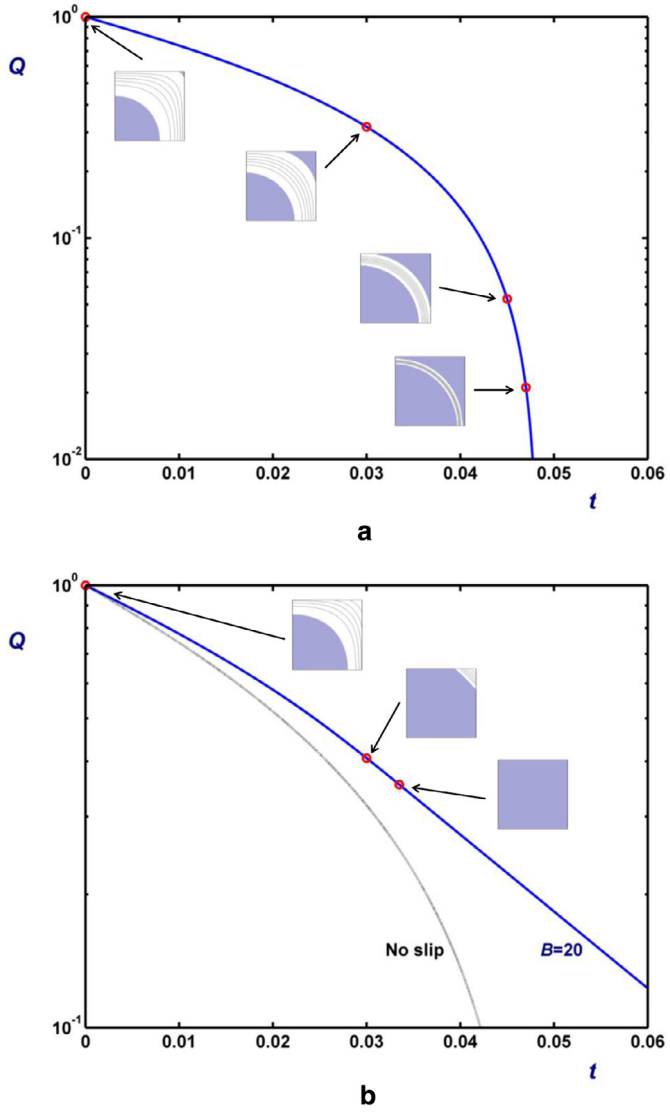

Fig. 23. Evolution of the volumetric flow rate in cessation of Bingham flow in a square duct for $Bn = 10$: (a) No wall slip; (b) Navier slip with $B = 20$.

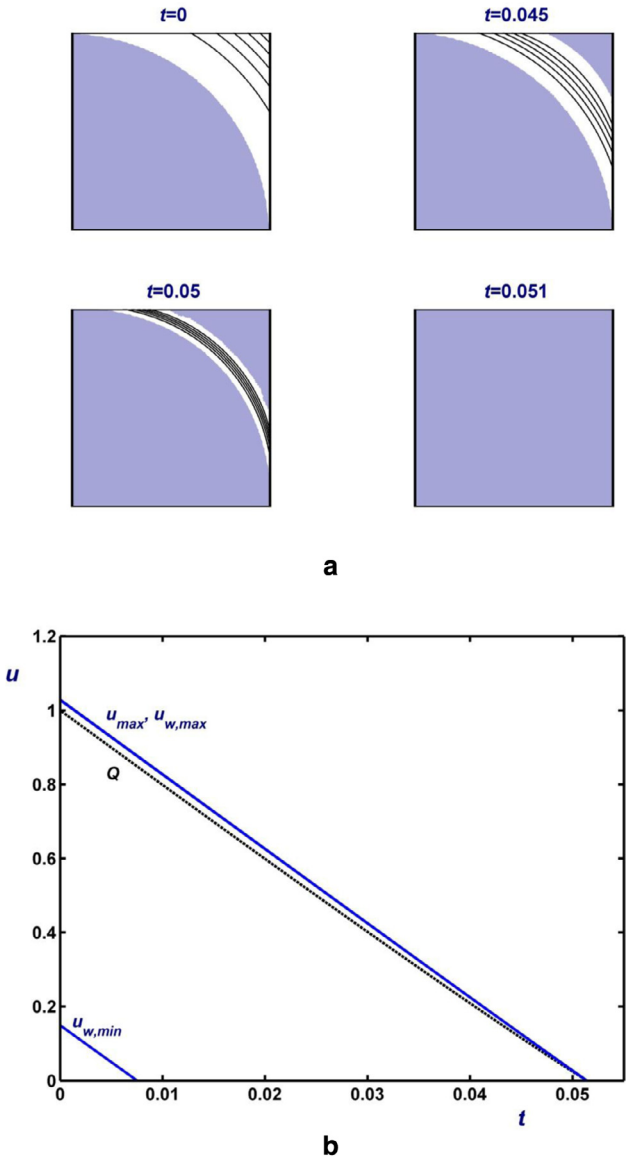

Fig. 24. Cessation of Bingham flow in a square duct with wall slip for $Bn = B_c = 10$ and $B = 0.1$: (a) Unyielded areas (shaded) and velocity contours; (b) Evolution of the volumetric flow rate (Q), the maximum velocity at the duct center (u_{max}), the maximum slip velocity at the middle of the duct wall ($u_{w,max}$), and the minimum slip velocity at the duct corner ($u_{w,min}$).

The computed values of the critical times for $B = 100$, 20 and 8 were $t_0 = 0.0459$, 0.0334 and 0.0073 with $u_{w0} = 0.0621$, 0.3553 and 0.8905, respectively.

Fig. 23 summarizes the main differences between the no-slip and Navier-slip cases. Application of the no-slip boundary condition leads to finite stopping times. A stagnant unyielded region appears at the corner which grows and merges with the central unyielded plug region (which also grows). In the presence of Navier slip, the fluid near the duct corners is always yielded; hence, no stagnant unyielded regions are observed. The central plug region grows, reaches the walls and then expands towards the corner to cover the entire flow domain at a certain critical time before cessation; beyond that time the plug velocity decays exponentially, i.e. the theoretical stopping time is infinite.

5.3. Slip with non-zero slip yield stress

As already mentioned, in this work we consider only the possibility of $Bn = B_c$. The initially applied pressure gradient is such that the initial volumetric flow rate is unity. As expected, the cessation solutions for non-zero slip yield stress combine features of both the Navier-slip and no-slip solutions.

Obviously, when the imposed pressure gradient is $G \le G_{c1}$, the no-slip boundary condition applies everywhere at all times and the results of Section 5.1 apply. If $G > G_{c2}$, then slip occurs everywhere only initially till a critical time t_c at which slip at the duct corners ceases. Hence initially there is no stagnant region near the corners as is the case when Navier slip is applied. For $t > t_c$, stagnant corner regions develop and grow to merge with the inner plug region, in a fashion similar to that of the no-slip case. The merging curve, however, does not have to lie inside the duct, since slip allows the possibility for the core plug region to reach the wall and expand towards the corners. This behavior of the solution is illustrated in Fig. 24 where results for of $Bn = B_c = 10$ and $B = 0.1$ are shown. Since the core plug expends to the wall the maximum slip velocity coincides with the maximum velocity. The evolution of the volumetric flow rate along with representative snapshots of the yield/unyielded regions is illustrated in Fig. 25. Finally, if $G_{c1} < G < G_{c2}$, when cessation starts there is already

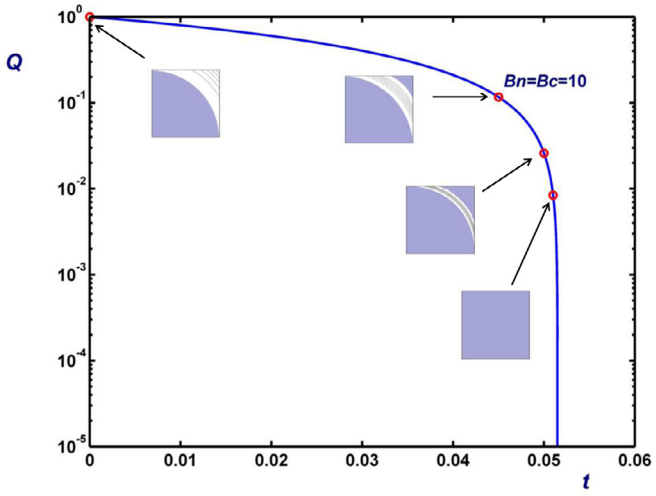

Fig. 25. Evolution of the volumetric flow rate in cessation of Bingham flow in a square duct for $Bn = B_c = 10$ and $B = 0.1$.

a stagnant region near the corners and the evolution of the flow is similar to that of Fig. 24 after the critical time t_c.

6. Conclusions

We have solved numerically the cessation of Bingham-plastic Poiseuille flow in a square duct with wall slip and non-zero slip yield stress using regularized versions of both the constitutive and the slip equations. The analytical solutions for the Newtonian flow have also been provided for the no-slip, the Navier-slip, and the non-zero slip yield stress cases. These served as good tests for the numerical code and the regularized slip equation.

The combined effects of viscoplasticity and slip on the flow have been investigated and the evolution of the unyielded regions has been studied. In the case of no-slip, the unyielded plug core and the corner stagnant zones grow during cessation and merge inside the duct causing the flow to stop at a finite time. The numerical stopping times are in excellent agreement with the theoretical estimates of Glowinski [15]. It has been demonstrated that when Navier slip is applied there are no stagnant regions near the duct corners. The plug core grows during cessation reaching the wall and continues growing towards the corners and the shrinking yielded corner region acquires the shape of an equilateral orthogonal triangle. Eventually the velocity becomes flat at a finite time before complete cessation. A simple analytical expression describes the decay of the flat velocity. This is exponential and thus the theoretical stopping time is infinite. Finally, when the slip yield stress is non-zero, the cessation of the flow depends on the value of the pressure gradient corresponding to the initial condition. When $G \leq G_{c1}$, the no-slip time-dependent solution applies. When the initial condition corresponds to a pressure gradient in the intermediate regime ($G_{c1} < G < G_{c2}$), there occurs partial wall slip and there are stagnant regions at the corners initially. These grow and merge with the expanding plug core in a fashion similar to that of the no-slip case. When $G \geq G_{c2}$, slip occurs everywhere initially; as a result, there are no stagnant regions near the duct corners. These appear only when slip at the duct corners ceases at the critical time t_c. After this critical time, the flow evolves as in the intermediate regime.

The regularized models generally provide satisfactory approximations of the ideal discontinuous equations provided that the regularization parameters are sufficiently high. Their performance, however, becomes problematic not only when the velocity is close to zero but also when it is almost flat. The latter phenomenon is encountered with Bingham fluids when Navier slip is applied, i.e. when the slip yield stress is zero; the velocity becomes plug at a finite critical time before complete cessation and then decays exponentially.

A straightforward extension of the present work is the solution of the Herschel–Bulkley flow in a duct of rectangular cross section with wall slip, allowing the possibility of the slip yield stress being different from the yield stress, as in Ref. [13]. The study of the start-up flow in order to verify the jerk wave hypothesis for the motion of the yield surfaces, as suggested by Huilgol [21], is also of interest.

References

[1] Y. Damianou, G.C. Georgiou, Viscoplastic Poiseuille flow in a rectangular duct with wall slip, J. Non-Newtonian Fluid Mech. 214 (2014) 88–105.
[2] M.M. Denn, Extrusion instabilities and wall slip, Ann. Rev. Fluid Mech. 33 (2001) 265–287.
[3] Y. Damianou, G.C. Georgiou, I. Moulitsas, Combined effects of compressibility and slip in flows of a Herschel–Bulkley fluid, J. Non-Newtonian Fluid Mech. 193 (2013) 89–102.
[4] J.M. Piau, Carbopol gels: Elastoviscoplastic and slippery glasses made of individual swollen sponges: Meso- and macroscopic properties, constitutive equations and scaling laws, J. Non-Newtonian Fluid Mech. 144 (2007) 1–29.
[5] C. Métivier, A. Magnin, The effect of wall slip on the stability of the Rayleigh-Bénard Poiseuille flow of viscoplastic fluids, J. Non-Newtonian Fluid Mech. 166 (2011) 839–846.
[6] P. Ballesta, G. Petekidis, L. Isa, W.C.K. Poon, R. Besseling, Wall slip and flow of concentrated hard-sphere colloidal suspensions, J. Rheology 56 (2012) 1005–1037.
[7] J.R.A. Pearson, C.J.S. Petrie, On the melt-flow instability of extruded polymers, in: Proceedings of the 4th International Congress on Rheology, 3, 1965, pp. 265–283.
[8] R.R. Huilgol, Fluid Mechanics of Viscoplasticity, Springer-Verlag, Berlin, 2015.
[9] R. Glowinski, A. Wachs, On the numerical simulation of viscoplastic fluid flow, in: R. Glowinski, J. Xu (Eds.), Handbook of Numerical Analysis : Numerical Methods for Non-Newtonian Fluids, 16, Elsevier, 2011, pp. 483–717.
[10] N.J. Balmforth, I.A. Frigaard, G. Ovarlez, Yielding to stress: recent developments in viscoplastic fluid mechanics, Annu. Rev. Fluid Mech. 46 (2014) 121–146.
[11] T.C. Papanastasiou, Flows of materials with yield, J. Rheology 31 (1987) 385–404.
[12] E. Mitsoulis, Flows of viscoplastic materials: models and computations, Rheol. Rev. 2007 (2007) 135–178.
[13] N. Roquet, P. Saramito, An adaptive finite element method for viscoplastic flows in a square pipe with stick-slip at the wall, J. Non-Newtonian Fluid Mech. 155 (2008) 101–115.
[14] Y. Damianou, M. Philippou, G. Kaoullas, G.C. Georgiou, Cessation of viscoplastic Poiseuille flow with wall slip, J. Non-Newtonian Fluid Mech. 203 (2014) 24–37.
[15] R. Glowinski, Numerical Methods for Nonlinear Variational Problems, Springer-Verlag, New York, 1984.
[16] R.R. Huilgol, B. Mena, J.-M. Piau, Finite stopping time problems and rheometry of Bingham fluids, J. Non-Newtonian Fluid Mech. 102 (2002) 97–107.
[17] E.A. Muravleva, L.V. Muravleva, Unsteady flows of a viscoplastic medium in channels, Mech. Solids 44 (2009) 792–812.
[18] R. Haberman, Elementary applied partial differential equations, with Fourier series and boundary value problems, 2 Edition, Prentice-Hall, Englewood Cliffs NJ, 1987.
[19] C. Fan, Unsteady-laminar incompressible flow through rectangular ducts, ZAMP 16 (1965) 351–360.
[20] G. Kaoullas, G.C. Georgiou, Newtonian Poiseuille flows with slip and non-zero slip yield stress, J. Non-Newtonian Fluid Mech. 197 (2013) 24–30.
[21] R.R. Huilgol, On the description of the motion of the yield surface in unsteady shearing flows of a Bingham fluid as a jerk wave, J. Non-Newtonian Fluid Mech. 165 (2010) 65–69.